Masuyama *et al. Robomech J* (2021) 8:21
https://doi.org/10.1186/s40648-021-00208-2

ROBOMECH Journal

RESEARCH ARTICLE Open Access

Force display control system for simultaneous 3-axis translational motion in surgical training simulator for chiseling operation

Kentaro Masuyama[1*], Yoshiyuki Noda[2], Yasumi Ito[2], Yoshiyuki Kagiyama[2] and Koichiro Ueki[3]

Abstract

The present study proposes an advanced force display control system for a surgical training simulator with virtual reality. In oral and orthopedic surgeries, a surgeon uses a chisel and mallet for chiseling and cutting hard tissue. To enable the representation of force sensation for the chiseling operation in a virtual training simulator, the force display device has been constructed with the ball-screw mechanism to obtain high stiffness. In addition, two-degrees-of-freedom (2DOF) admittance control has been used to react instantaneously to the impactive force caused by pounding with the mallet. The virtual chiseling operation was realized by the force display device with a single axis in the previous studies. In the current study, we propose the design procedure for the force display control system with the 2DOF admittance control approach to virtual operation in three-dimensional space. Furthermore, we propose the design method for the PD controller with imperfect derivative using frequency characteristics for the 2DOF admittance control system. The efficacy of the proposed control system is verified through the virtual experience from manipulating the chisel using the developed force display device in the current study.

Keywords: Surgical training simulator, Virtual reality, Force display device, Chiseling, 2DOF admittance control

Introduction

Surgical training simulators enhanced by virtual reality have been developed to enable surgeons to efficiently acquire and improve their surgical skills. The virtualized environment is created by vision, hearing and force sensory immersion so that the surgeons can practice surgical procedures repeatedly and safely with high realistic sensation [1–6]. In virtual training systems for soft tissue such as the brain [7], organs and so on [8–10], force display devices have used either the serial link mechanism [11–14] or the parallel mechanism [15–18]. These force display devices allow for increased responsiveness by lightening the moving parts, resulting in a precise sensation of contact with the soft tissue.

In oral and orthopedic surgeries, surgeons operate hard tissue such as bone and tooth using a drill, saw and so on. Virtual training simulators for operating with the drill [19–21] or saw [22–24] have been proposed in previous studies. Large operational forces are applied to the force display device. It is difficult to withstand such large operational forces in the force display devices of the training simulator for the soft tissue. Specifically, in surgical operation using a chisel and mallet, large impactive forces are applied for cutting and excising pieces of bones. Therefore, the force display device used the surgical operation of hard tissue has required high stiffness to withstand the impactive force. Furthermore, high responsiveness is also demanded to react

*Correspondence: g19dts07@yamanashi.ac.jp
[1] Integrated Graduate School of Medicine, Engineering, and Agricultural Sciences, University of Yamanashi, 4-3-11 Takeda, Kofu-shi, Yamanashi 400-8511, Japan
Full list of author information is available at the end of the article

instantaneously to the operational impactive force for representing the hard contact sensation.

In our previous studies [25, 26], the force display device was constructed using the ball-screw mechanism to achieve high stiffness, and the two-degree-of-freedom (2DOF) admittance control was proposed so that the device can react instantaneously to the impactive forces. It was verified that the reaction force by employing the 2DOF admittance control could precisely display the output of a virtual model.

In another previous study [27], the virtual model was designed to represent the chiseling operation with high realistic sensation by pounding with the mallet. This model was consisted of the spring-mass-damper system with the moving equilibrium point. The parameters in the virtual model were identified by comparing the real chiseling operation to the operational force detected by a force sensor. The efficacy of the 2DOF admittance control system used in the proposed virtual model was verified by subjective evaluation through the virtual experience to chisel the hard tissue. However, in these previous studies, the control systems for displaying the reaction force were designed only for the motion on a single axis. The force display control system should be extended to the motion in three-dimensional space. When contacting the hard tissue with a small operating force, the tip of the chisel can be moved to the surface of the hard tissue. On the other hand, it is difficult to move the tip of the chisel to different directions from the stabbing direction when stabbing the chisel to the hard tissue with a large operating force. As seen above, the motion of the chisel can be constrained depending on the situations in three-dimensional space.

Furthermore, the feedback controller in the 2DOF admittance control system was designed by the PD controller with imperfect derivative. However, the parameters in the PD controller were derived by the empirical rule. It is necessary to derive the parameters systematically.

In this study, the design method for the force display control system with the 2DOF admittance control approach to the virtual chiseling operation in three-dimensional space is proposed. In the proposed approach, the virtual model for representing the force sensation is constructed for three situations of manipulating the chisel in the air, contacting the hard tissue, and stabbing into the hard tissue. Furthermore, the design procedure for the parameters in the PD controller with imperfect derivative using frequency characteristics is also proposed for designing systematically the feedback controller with increasing a high-frequency gain and suppressing the vibrational motion. The efficacy of the proposed control system is verified through the virtual experience manipulating the force display device.

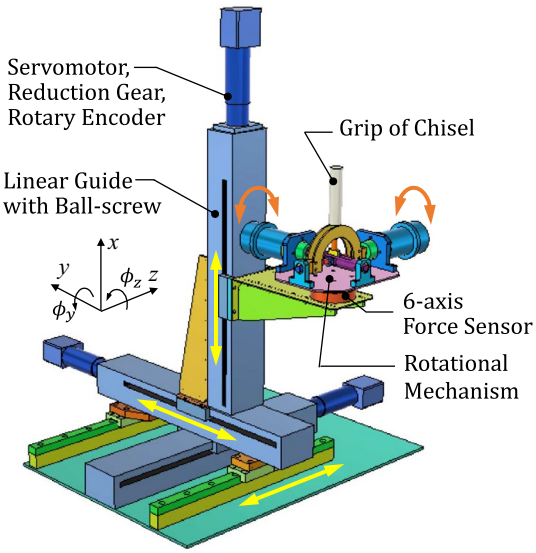

Fig. 1 Force display device for surgical training simulator with chiseling operation

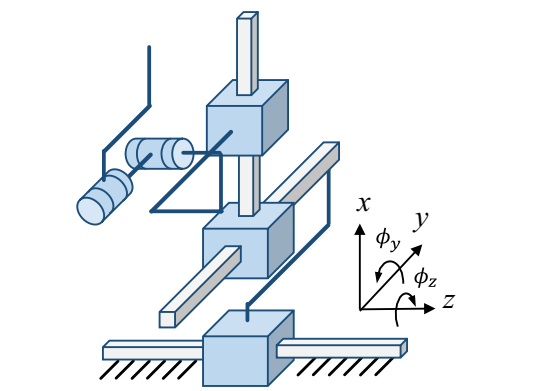

Fig. 2 Skeleton diagram of force display device for surgical training simulator

Methods

Force display device

Figure 1 shows an illustration of the force display device in the virtual surgical simulator used in the current study. Figure 2 shows the skeleton diagram of this force display device. This notation of the diagram is referred in [28]. This device has 5DOF motion, and the chisel as the end effector can move in the x-, y- and z-directions and rotate in the ϕ_y- and ϕ_z-directions. The chiseling translational

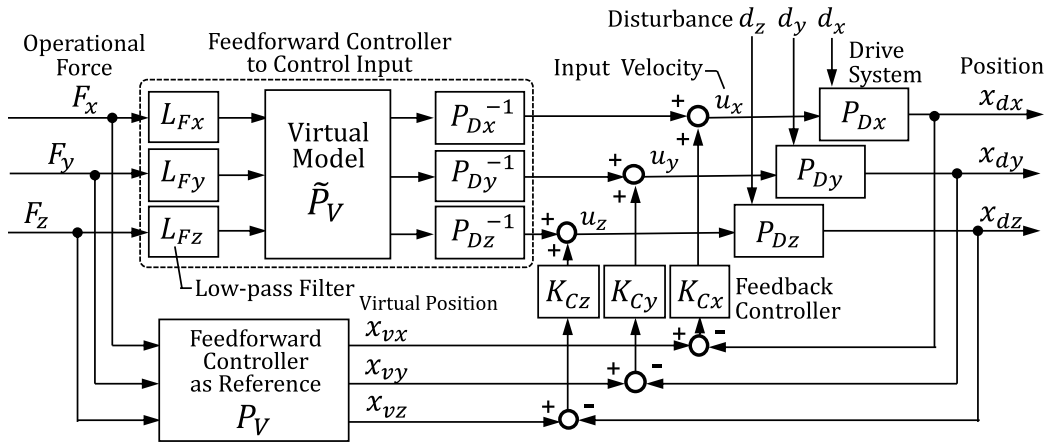

Fig. 3 Block diagram of 2DOF admittance control

Table 1 Specifications of force display device

	Translational motion	Rotational motion
Display force	Max. 100 N	Max. 5.49 Nm
Velocity	Max. 0.76 m/s	Max. 1181 deg/s
Distance or angle	290 mm	65 deg

motions in the force display device are realized using the ball-screw mechanism (THK, SKR46). In the force display device, the ball-screw mechanism as a translational mechanism is located on the bottom as shown in Fig. 2. This mechanism whose allowable moment in the linear table is 579 Nm has more than enough stiffness to resist the maximum impactive force. The rotational mechanism is located on the edge of the device for reducing the load to it. The torque-loaded components in the rotational mechanism are designed to withstand the impactive force. These can be maintained with the deflection of less than 1 mm. The rotational mechanism is fixed rigidly to the linear table of the ball-screw mechanism. Therefore, the total stiffness of the force display device is enough to the maximum impactive force.

Table 1 shows the specifications of the force display device. In the previous studies, it was clarified that the cutting force by scratch using the tool bit [29, 30] and by drill [31, 32] were less than 100 N. However, the chiseling force using to the hard tissue is not sure in previous studies. In the preliminary experiments, we measured the chiseling force using a force plate. As the results, the maximum chiseling force was from 30 to 70 N. We designed the force display device which can withstand the maximum impactive force, 100 N.

Table 2 Parameters on drive system

Direction	T_m / ms	K_m
x-axis	4.93	1.00
y-axis	4.91	1.00
z-axis	5.76	1.00

The previous study [33] showed that the maximum tangential velocities of human arm were from 0.7 to 1.3 m/s. However, it is difficult to realize both of high-speed motion and large displayed force in the force display device. Therefore, we set the requirement of the maximum velocity to over 0.7 m/s in this study.

The servomotors installed into the ball-screw mechanism are MAXON EC45 on each axis. The servomotors using to the rotational mechanism are EC60flat in ϕ_y-, ϕ_z-directions. The reduction gears mounted each servomotor are GP42C (3.5:1) in *x*- and *y*-directions, GP62 110499 (5.2:1) in *z*-direction, and GP52C (19:1)ϕ_y-, ϕ_z -directions, respectively. These specifications of the force display device satisfy to create realistic surgical sensations when using the chisel.

A six-axis force sensor (Leptrino, 080YA501) is installed at the bottom of the rotational mechanism. The rated capacities of measurable force and torque are 500 N and 20 Nm on each axis, respectively. The resolutions of those are 0.125 N and 0.005 Nm, respectively. Therefore, the impactive force applied to the end effector by an operator can be measured by the force sensor. And, it

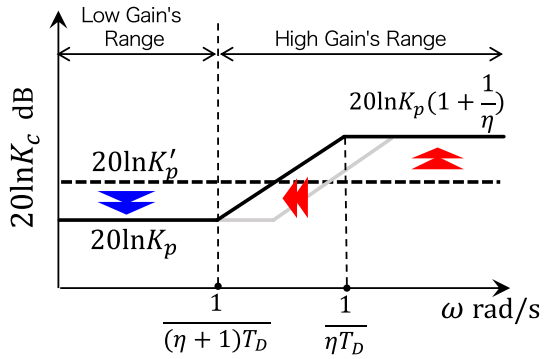

Fig. 4 Design of PD controller with imperfect derivative in frequency domain

Table 3 Parameters on feedback controllers

Direction	α	K_P	T_D	η
x-axis	1.5	4.7	0.020	0.50
y-axis	1.5	3.7	0.013	0.40
z-axis	1.5	4.0	0.015	0.60

also enables to measure suitably the operational force to a lightweight object such as a chisel.

Force display control system

To create the force sensory immersion with high realistic sensation, the motion of the drive system requires precise tracking of the output of the virtual model. However, if the conventional admittance control, which consists of only feedback control, is applied to the force display device, the responsiveness of the force display device with the ball-screw mechanism used in the current study can be reduced by increasing the mass of moving parts.

Therefore, the 2DOF admittance control extended from the traditional admittance control system to 2DOF control approach by combining the feedforward and feedback controls [34] is applied to the drive system for instantaneously reacting and precisely tracking the output of the virtual model. The feedforward controller to control input provides instantaneous responsiveness to the drive system. And, the feedback controller enhances the tracking performance even with disturbance and modeling error of the drive system. Figure 3 shows the

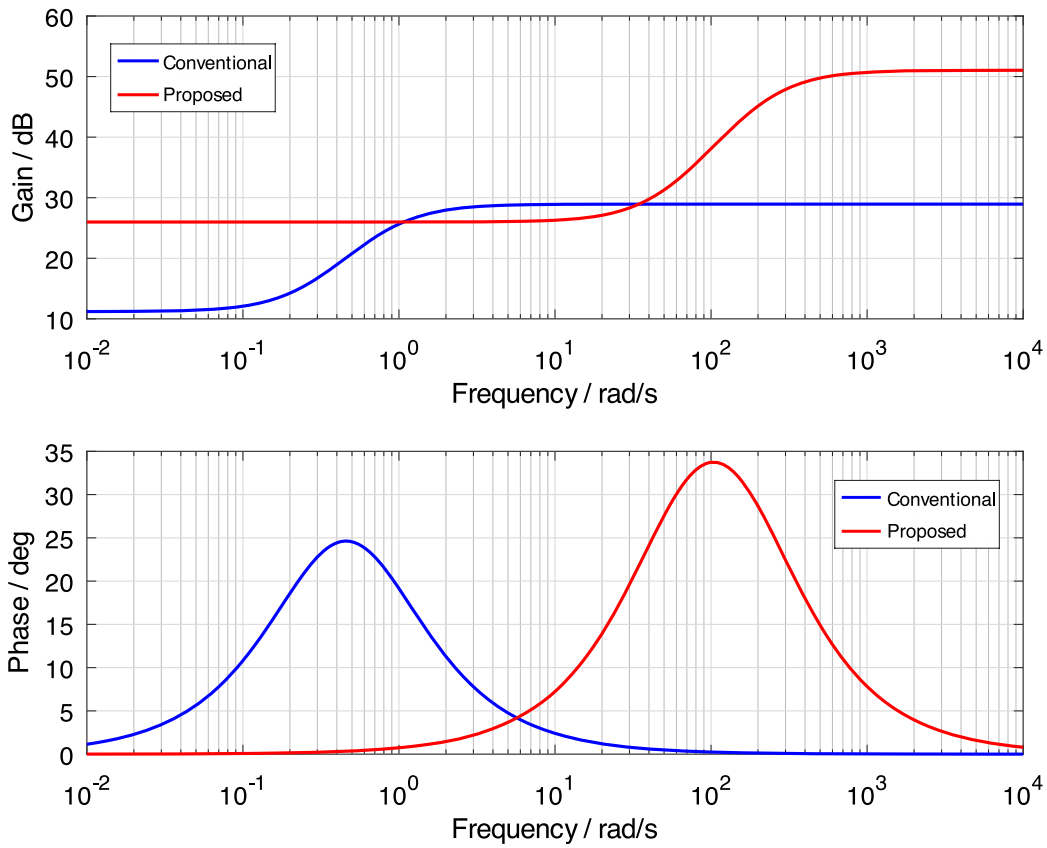

Fig. 5 Bode diagram of comparison with conventional PD control [27] in *y*-axis

2DOF admittance control installed in the force display device, where F is the operational force measured by the force sensor, u is the input command, x_d is the position of the tip of the chisel and d is the disturbance. The mathematical representations of each block are described in the subsections below.

Drive system P_D

The velocity feedback control is implemented into the servomotor system on each axis. We assumed that the 3DOF translational motions and the 2DOF rotational motions are controlled independently. And, the drive systems of the translational motion can be represented simply as

$$\ddot{x}_{di} = \frac{1}{T_{mi}}\dot{x}_{di} + \frac{K_{mi}}{T_{mi}}u_i, \ (i = x, y, z), \tag{1}$$

where T_m is the time constant, K_m is the gain and i is the moving direction. The time constants and the gains in the three dimensions are identified as Table 2. The force caused by the motion of other axes such as Coriolis force is not taken into consideration in this study. Because the influence of that force is small due to the small angular velocities of chisel motion, and the disturbance can be suppressed by the servo drive system.

The servomotors used in the rotational mechanism is used to display the reaction torque to rotate the chisel. The restraint in the chisel rotation caused by stabbing the chisel to the hard tissue and contacting the obstacles in the radial direction of the chisel can be realized by displaying the reaction torque. However, in this study, we focus on the design of force display control system for the translational motion of chisel operation. Therefore,

Table 4 Comparison with gain and break frequency of feedback controller in *y*-axis

Method	Gain		Break freq.	
	Low freq.	High freq.	Low freq.	High freq.
	dB	dB	rad/s	rad/s
Conv. [27]	11.20	28.94	0.2941	0.7143
Proposed	25.99	51.04	55.56	194.4

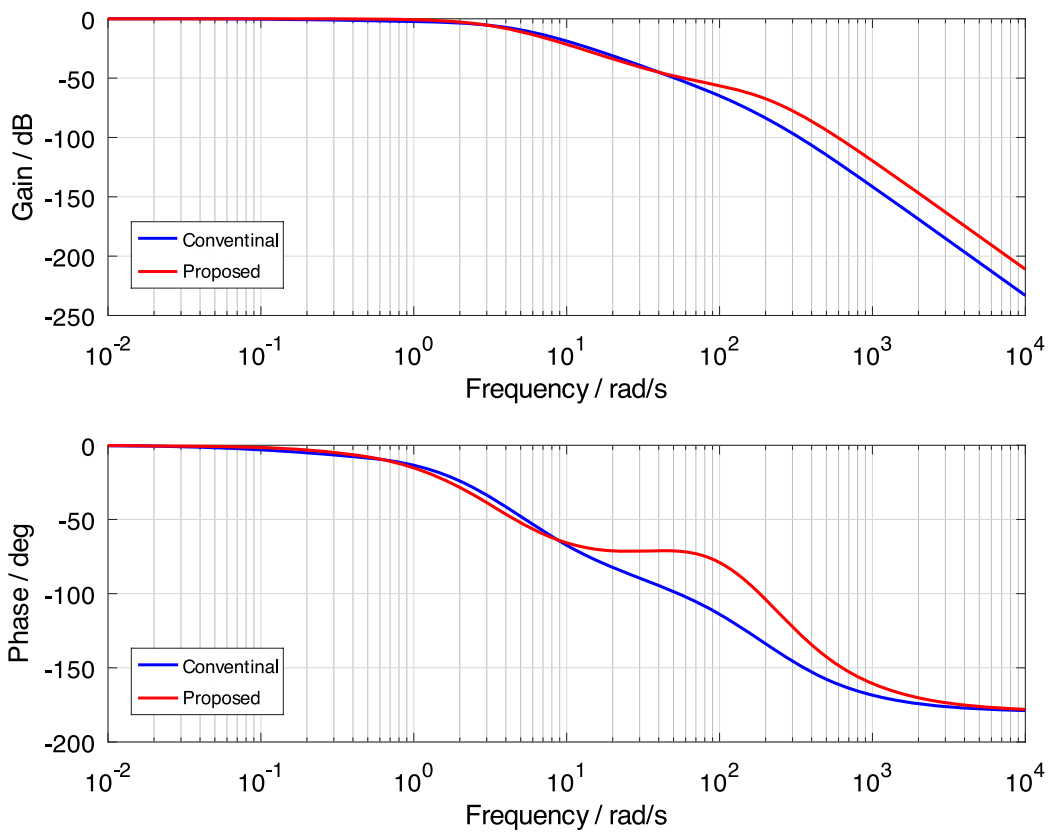

Fig. 6 Bode diagram of closed-loop feedback control system from x_{vy} to x_{dy} in *y*-axis

Table 5 Cut-off angular frequencies in low-pass filters applied on *x*-, *y*- and *z*-axis.

Direction	ω_f / rad/s
x-axis	23.0
y-axis	6.0
z-axis	3.0

we do not discuss the reaction torque display to the chisel rotation.

Feedback controller K_C

According to the analysis of the 2DOF admittance control system in the previous study [27], the feedback controller K_C needs to increase a high-frequency gain to track the output of the virtual model precisely. Therefore, the PD control is applied to the feedback controller. Then, the derivative term in the PD controller is represented by the imperfect differential calculus to suppress the sensor noise and the vibrational mode of the device. The transfer function of the PD controller can be represented as

$$\begin{aligned} K_{Ci}(s) =& \frac{U_{fbi}(s)}{E_i(s)} \\ =& K_{Pi}\left(1 + \frac{T_{Di}s}{\eta_i T_{Di}s + 1}\right), \quad (i = x, y, z), \end{aligned} \tag{2}$$

where s is the Laplace operator, K_P is the proportional gain, T_D is the derivative time and η is the derivative coefficient. These parameters are configured after the design of the feedforward controllers and the virtual model, as mentioned later. In the previous studies [27], the PD controller was designed using the empirical rule. In the present study, we propose the design procedure for the PD controller using the frequency characteristics. The gain plot of the PD controller is shown in Fig. 4.

In the design of the PD controller, first, the temporal proportional gain K'_P is increased while the vibrational motion in the device is suppressed within the allowed amplitude, and the derivative time T_D is zero as

$$\max K'_{Pi},\ (T_D = 0,\ U_{di} < U_o,\ i = x, y, z), \tag{3}$$

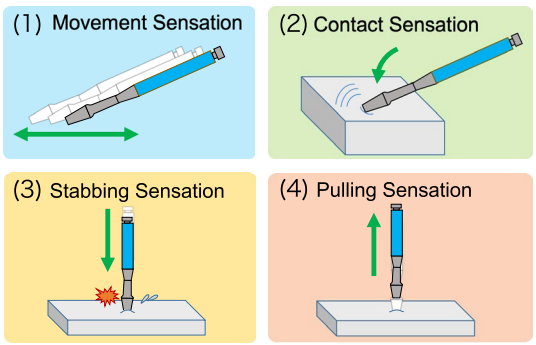

Fig. 7 Operational sensations between chisel and hard tissue

where U_o is set as the allowed amplitude of vibrational motion in the position of the end effector x_d, and U_d is the amplitude of the vibrational motion in the position of the end effector x_d. In the present study, the allowed amplitude U_o of the vibrational motion is set as $U_o = 1$ mm to have no adverse influence on the operational sensation. To suppress the vibrational motion, which can be increased by adding the derivative term, the proper proportional gain K_P can be designed as

$$K_{Pi} = \frac{K'_{Pi}}{\alpha_i},\ (\alpha_i > 1,\ i = x, y, z), \tag{4}$$

where α is the reduction factor. The tracking performance of the drive system can be decreased by increasing the reduction factor α. We recommend a small reduction factor from 1 to 2 to maintain tracking performance.

In the next step, the temporal derivative time T'_D is increased while suppressing the vibrational motion under the allowed amplitude. Here, the temporal derivative coefficient is set as $\eta' = 1/(\alpha - 1)$. The break frequency over which the gain is increased is diminished by increasing the derivative time. The temporal derivative time derived in this step is represented as

$$\max T'_{Di},\ (\eta'_i = \frac{1}{\alpha_i - 1},\ U_{di} < U_o,\ i = x, y, z). \tag{5}$$

Finally, the derivative coefficient η is reduced to increase the high gain's range, and the proper derivative time T_D can be obtained as

Table 6 Parameters of virtual model on situations

	Situation	Model parameters				Generalized parameters			
		m_v / kg	c_v / kg/s	k_v / N/m		ω_n / rad/s	ζ	ω_c / rad/s	K
(a)	Contacting har tissue	100	1.2×10^4	3.6×10^5	(a)	60	1	–	0.01
(b)	Manipulating in air	2	20	0	(b)	–	–	10	0.5

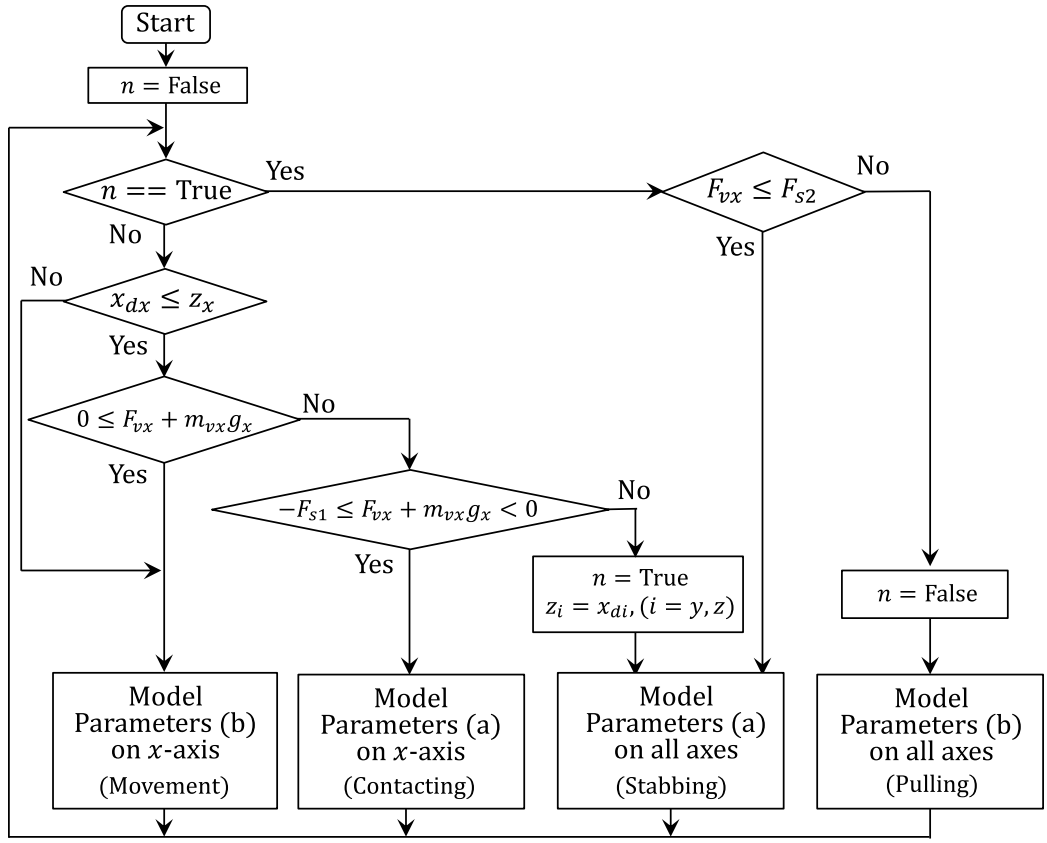

Fig. 8 Switch conditions for parameters of virtual model

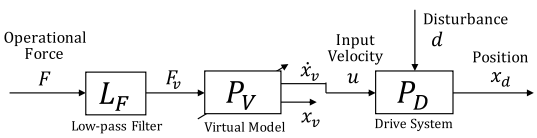

Fig. 9 Block diagram of conventional admittance control

$$\min \eta_i, \quad (T_{Di} = \frac{\eta_i' + 1}{\eta_i + 1} T_{Di}',\ U_{di} < U_o,\ i = x, y, z). \tag{6}$$

The derivative time T_D varies depending on the derivative coefficient η, whereas the low break frequency does not vary according to the constraint in Eq. (6). In the present study, Table 3 shows the reduction factor α, the proportional gain K_P, the derivative time T_D and the derivative coefficient η.

Figure 5 shows the frequency characteristics of the proposed PD controller. For comparison purpose, we also show the PD controller designed using the conventional approach [27]. In this figure, the upper and lower graphs represent the gain and phase characteristics, respectively. The blue and red lines represent the characteristics of the conventional and proposed PD controllers, respectively. The low- and high-frequency gains and these break frequencies are shown in Table 4.

Figure 6 shows the closed-loop characteristics of the feedback control systems from x_{vy} to x_{dy} in the frequency domain. The arrangement of graphs is the same as in Fig. 5. The blue and red lines represent the characteristics of the conventional PD control and proposed PD control, respectively. The proposed PD control system has a higher high-frequency than the conventional PD control system. Therefore, the responsiveness of the drive system to the impactive force can be improved by the proposed PD control system.

In the design procedure of the proposed PD controller, the allowed amplitude of the vibrational motion is given as the boundary condition for suppressing the vibrational motion within 1 mm. Thus, it is difficult to increase the high frequency gain or decrease the low break frequency to the proposed PD controller as shown in Table 4. On

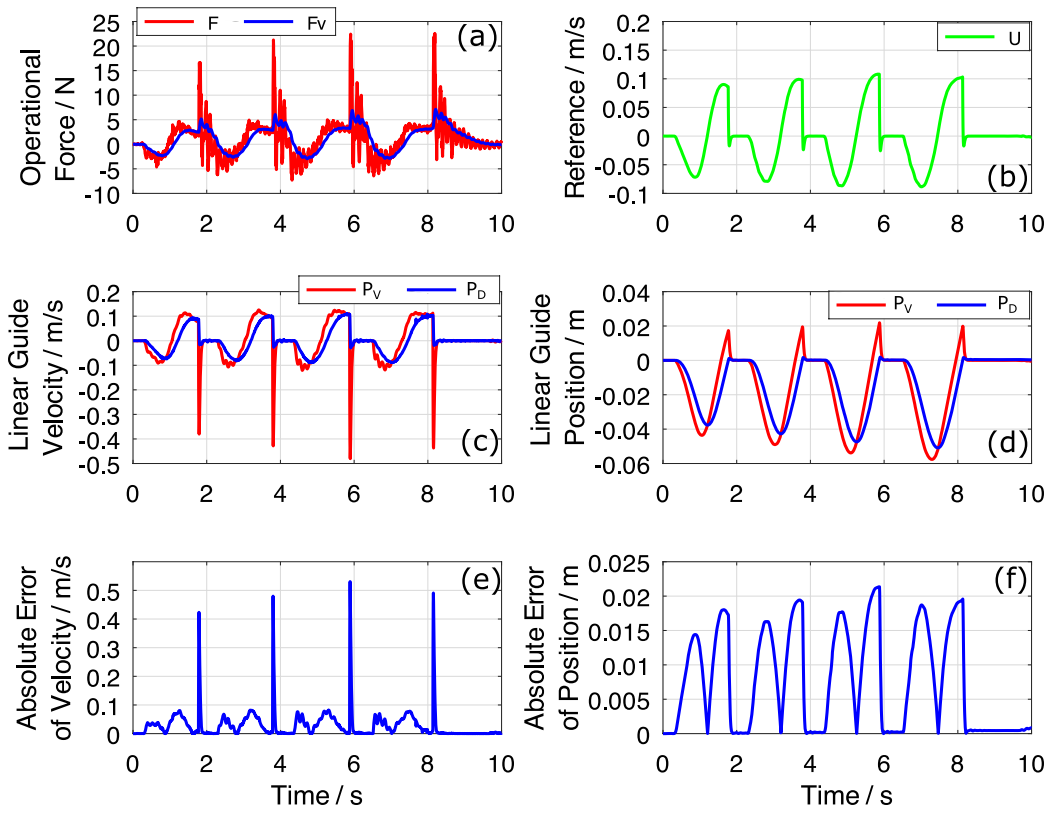

Fig. 10 Experimental results using admittance control in *y*-axis

the basis of these results, we confirmed that the parameters in the proposed PD control were designed appropriately for tracking precisely the output of the virtual model and suppressing the vibrational motion.

Feedforward controller as reference input,P_V

The feedforward controller as the reference input to the feedback control system is constructed with the proper virtual model P_V to create the appropriate chiseling environment. The virtual model P_V, which is the source of the force representation for creating the operational sensation, represents the dynamics relationship between the operational force and the tip position of the chisel. The dynamics of the virtual model is represented as

$$m_{vi}\ddot{x}_{vi} + c_{vi}\dot{x}_{vi} + k_{vi}(x_{vi} - z_i) = F_i + m_{vi}\gamma g_i, \quad (i = x, y, z), \tag{7}$$

where x_v is the position of the tip of the chisel in the virtual model, z is the equilibrium point and g is the gravitational acceleration. The model parameters m_v, c_v and k_v are the mass, viscosity coefficient and spring constant in the virtual model, which are represented as the spring-mass-damper system, respectively. The design procedure of these model parameters m_v, c_v and k_v is described in the next section. The gravitational acceleration is $g_x = -9.8\ \mathrm{m/s^2}$ in the x-axis, and other axes are $g_y, g_z = 0\ \mathrm{m/s^2}$. However, the addition of pure gravitational acceleration in the virtual model causes the overload of the motor in the force display device. Therefore, the safety coefficient γ is multiplied by the gravitational acceleration g. In the present study, the safety coefficient is set as $\gamma = 0.2$. The equilibrium point in the x-axis is set as $z_x = 0\ \mathrm{m}$.

Feedforward controller to control input, $L_F\tilde{P}_V P_D^{-1}$

The feedforward controller added to the control input of the feedback control system is constructed with the pseudo virtual model $\tilde{P}_V$, the low-pass filter L_F and the inverse model P_D^{-1} of the drive system to improve the responsiveness of the force display system. The low-pass

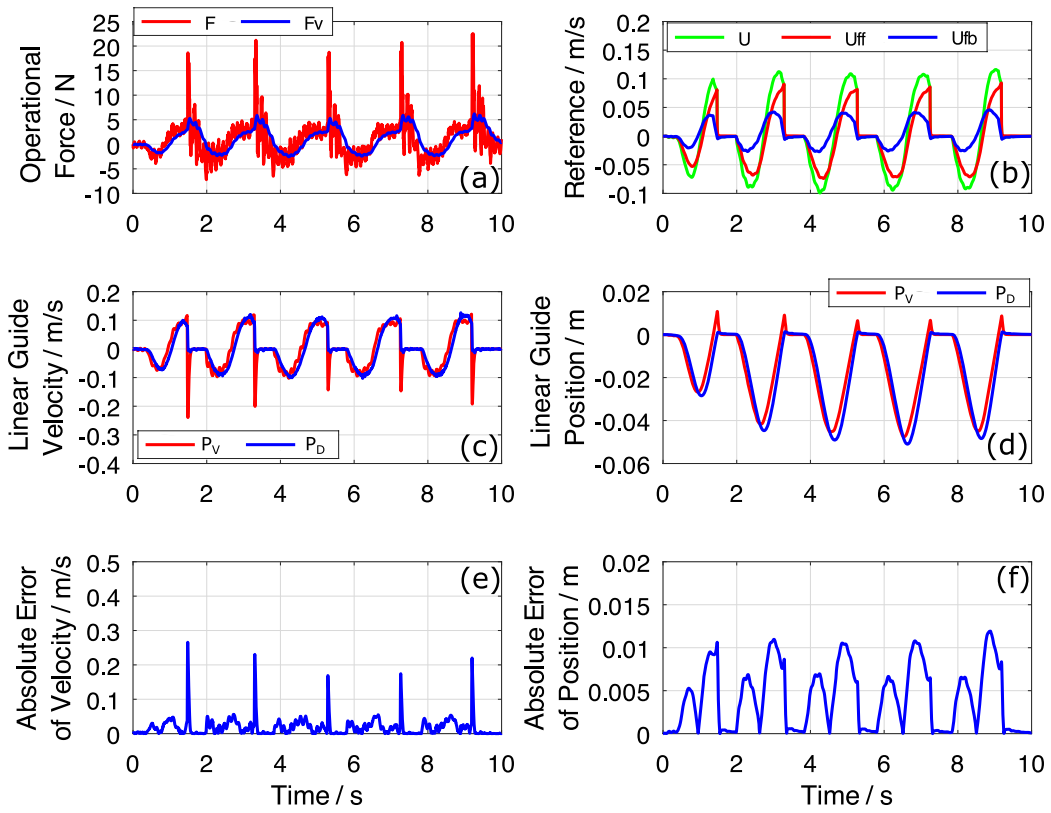

Fig. 11 Experimental results using 2DOF admittance control in *y*-axis

filter L_F is applied in front of the pseudo virtual model to suppress the sensor noise and is represented as

$$\dot{F}_{vi} = -\omega_{fi} F_{vi} + \omega_{fi} F_i, \ (i = x, y, z), \tag{8}$$

where F_v is the modified operational force through the low-pass filter. The low-pass filter parameter, ω_f is equal to the cut-off angular frequency. Table 5 shows the cut-off angular frequency in the filter applied to the control system on each axis. The low-pass filter was designed by making the cut-off angular frequency increase while the amplitude of the vibrational motion is suppressed with less than 1mm for reducing the signal loss of the measured forces adding to the pseudo virtual model and suppressing the vibrational motion. Therefore, the parameters in the low-pass filters were designed appropriately for getting better responsiveness of the force display device.

The pseudo virtual model $\tilde{P}_V$ in the feedforward controller to the control input is designed as

$$m_{vi}\ddot{x}_{vi} + c_{vi}\dot{x}_{vi} = F_{vi} + m_{vi}\gamma g_i, \ (i = x, y, z). \tag{9}$$

Since the feedforward controller to the control input is used to improve the responsiveness of the drive system and is required to avoid worsening the contact sensation on the hard tissue, the spring term has been removed from the virtual model P_V.

The inverse model of the drive system P_D^{-1} is implemented to suppress the response lag by the drive system, and is represented as the inverse of Eq. (1).

Parameters design of virtual model

Design of virtual model's parameters on situations

To represent the operational sensations such as the contact with the hard tissue and manipulation of the chisel freely in the air, the model parameters m_v, k_v and c_v in the virtual model can be varied in according to the situations. In the situation which the chisel is in contact with the hard tissue, the model parameters can be derived by transforming the virtual model of Eq. (7) to the generalized form as

$$\ddot{x}_{vi} + 2\zeta_i \omega_{ni} \dot{x}_{vi} + \omega_{ni}^2 x_{vi} = K_i F_i + \gamma g_i + \omega_{ni}^2 z_i, \ (i = x, y, z), \tag{10}$$

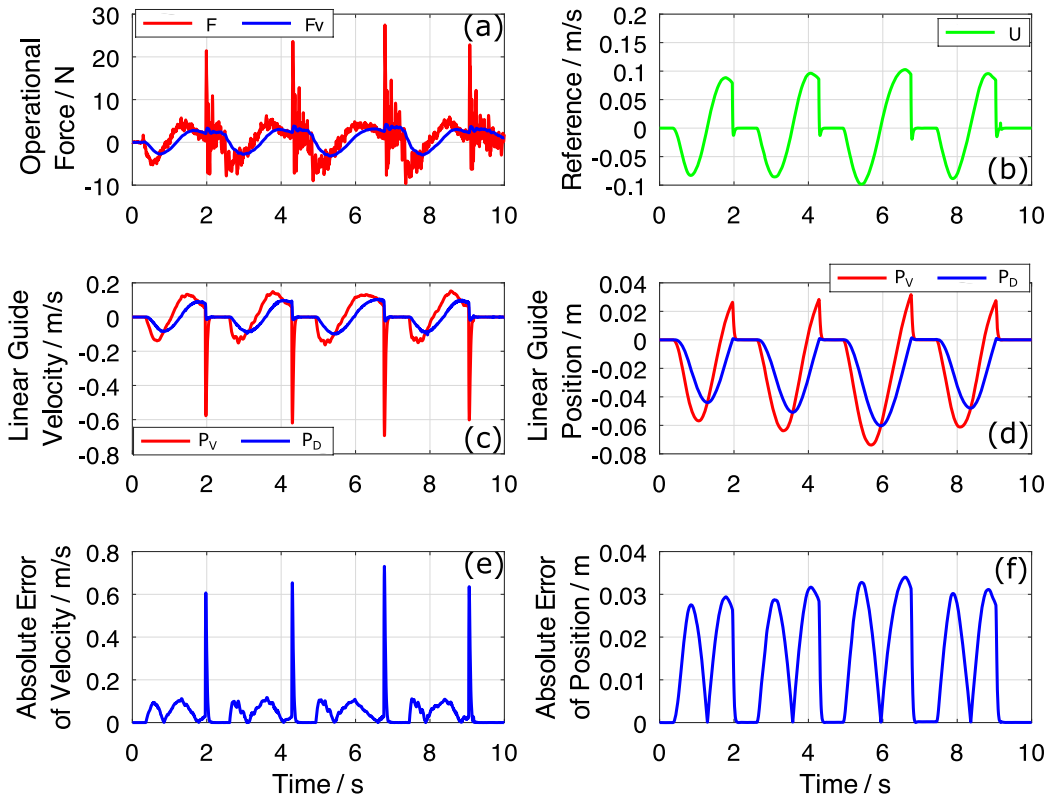

Fig. 12 Experimental results using admittance control in *z*-axis

where

$$\omega_{ni} = \sqrt{\frac{k_{vi}}{m_{vi}}}, \quad \zeta_i = \frac{c_{vi}}{2\sqrt{m_{vi}k_{vi}}}, \quad K_i = \frac{1}{m_{vi}}, \tag{11}$$

ω_n is the natural angular frequency, ζ is the damping ratio and K is the gain of the virtual model. The damping ratio is given as ζ=1 to suppress the vibration. To represent the situation in which there is contact with the hard tissue in the virtual model, the gain K is minified, and the natural angular frequency ω_n is increased while they are required to satisfy $U_{di} < U_o$ to suppress the vibrational motion.

In the situation where the chisel is manipulated in the air, the spring term is not required. Therefore, the virtual model can be represented as a first-order lag system with the integrator as

$$\ddot{x}_{vi} + \omega_{ci}\dot{x}_{vi} = K_i F_i + \gamma g_i, \quad (i = x, y, z), \tag{12}$$

where

$$\omega_{ci} = \frac{c_{vi}}{m_{vi}}, \quad K_i = \frac{1}{m_{vi}}. \tag{13}$$

To represent the situation where the chisel is manipulated in the air, the gain K is increased, and the cut-off angular frequency ω_c is decreased while satisfying $U_{di} < U_o$ to suppress the vibrational motion.

In the current study, we designed the virtual model's parameters for each situation, as shown in Table 6. The rows (a) and (b) in Table 6 show the model parameters for representing the situations of having contact with

Table 7 Maximum absolute errors of positions between virtual model and drive system

	Admittance control	2DOF Admittance control	
Direction		**Conv. PD [27]**	**Proposed PD**
x-axis	4.11 mm	–	1.70 mm
y-axis	21.4 mm	17.7 mm	12.1 mm
z-axis	34.0 mm	–	16.7 mm

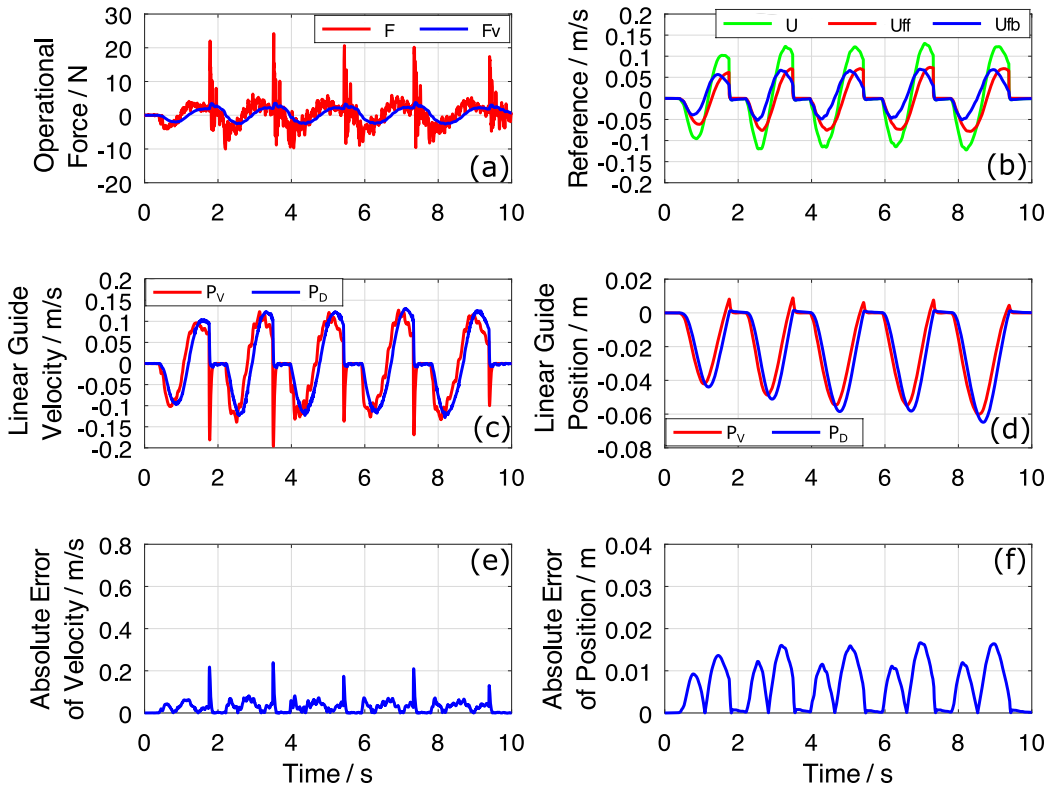

Fig. 13 Experimental results using 2DOF admittance control in *z*-axis

the hard tissue and manipulating the chisel in the air, respectively.

Switch of virtual model's parameters with changing situation

The model parameters represented in previous subsection are switched depending on the situation as shown in Fig. 7. The switch conditions of the model parameters for manipulating the chisel in the air and having contact with the hard tissue are designed independently of the translational motion of the three axes. On the other hand, to represent the situation of stabbing the tip of the chisel to the hard tissue when large operational force is applied, the virtual model is needed to design according to the motion of three-dimensional space. In the current study, we proposed the design procedure that enables the virtual model to represent the free manipulation sensation, contact sensation, stabbing sensation and pulling sensation created by an up-down motion.

The contact sensation on the hard tissue is created by switching the model parameters from (b) to (a) on each axis when small operational force is applied. In the situation where the operational force in the contact direction is larger than the threshold value F_{s1}, the stabbing sensation is created by switching the model parameters from (b) to (a) in all axes to represent the restrained situation. The pulling sensation is created by switching the model parameters from (a) to (b) when the operational force to the opposite direction is larger than the threshold value F_{s2}. Figure 8 shows these switching conditions of the model parameters, where F_v is the modified operational force through the low-pass filter L_F. The boolean variable, $n =$ true, indicates that the tip of the chisel is stabbing the hard tissue.

In the present study, the angle of the chisel is not considered during switching for the stabbing sensation, and the threshold values are set as $F_{s1} = 20$ N and $F_{s2} = 10$ N.

Experimental results

Comparison between force display control methods

The efficacy of the proposed 2DOF admittance control applied on each axis is verified by comparing it with the conventional admittance control [27]. Figure 9 shows

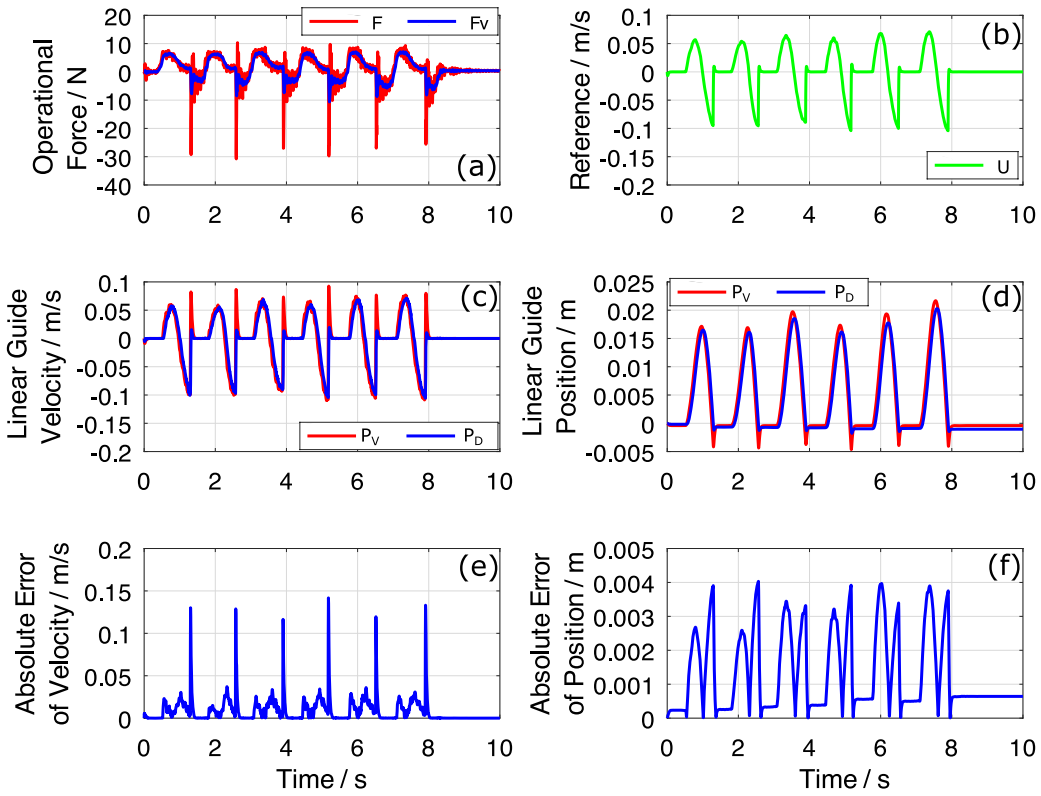

Fig. 14 Experimental results using admittance control in *x*-axis

the block diagram of the conventional admittance control. The cut-off angular frequency ω_f of the low-pass filter for suppressing the vibrational motion is obtained, as shown in Table 5 on each axis. To confirm the representation of the output of the virtual model, we evaluate the error between the outputs of the proper virtual model P_V and the movement of the chisel through the drive system P_D.

Figure 10 shows the experimental results using the conventional admittance control for the movement sensation in the air and the contact sensation in the *y*-axis, where (a) shows the operational force measured by the force sensor, (b) is the input command to the drive system, (c) and (e) are the velocity and the position of the tip of the chisel, respectively, and (d) and (f) are the absolute error of the velocity and the position between the virtual model and the drive system, respectively. In the free horizontal manipulation of the chisel using the conventional control approach, the maximum absolute error of the position is 0.021 m. Figure 11 shows the experimental results using the proposed 2DOF admittance control in the *y*-axis. The graphs in Fig. 11 have the same arrangement as those in Fig. 10. The absolute error of the position is less than 0.012 m.

Figures 12 and 13 show similar experimental results on the *z*-axis, whereas Figs. 14 and 15 show similar experimental results on the *x*-axis. Therefore, the proposed control system improved the realization of the virtual model for the free manipulation and the contact sensation.

Comparison between feedback controllers in 2DOF admittance control system

The tracking performance of the 2DOF admittance control with the conventional PD control [27] was compared with that of the proposed PD control using the chisel manipulation with the force display device. Figure 16 shows the experimental results by the force display device implementing the 2DOF admittance control with the conventional PD control; this figure is the results of the chisel motion on the *y*-axis. The chisel was manipulated, as described in the previous subsection. Therefore, we

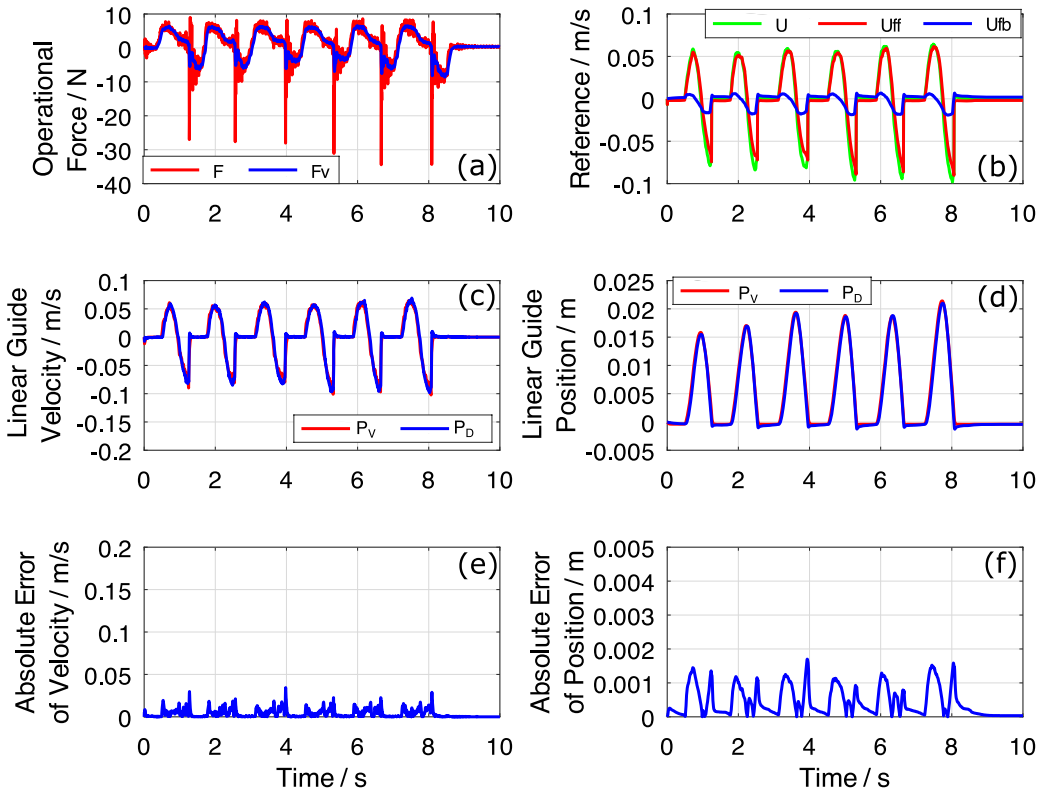

Fig. 15 Experimental results using 2DOF admittance control in *x*-axis

refer to Fig. 11 for the experimental results of the 2DOF admittance control system with the proposed PD control.

Figures 11f and 16f show that the tracking error of the conventional PD control is larger than that of the proposed PD control. Therefore, the force display device implementing the 2DOF admittance control with the proposed PD control can precisely represent the output of the virtual model.

Stabbing sensation

Figure 17 shows the experimental results of the stabbing operation using the proposed 2DOF admittance control. Graphs (a), (b) and (c) show the operational forces for operating the chisel on the *x*-, *y*- and *z*-axes, respectively. From 1.7 to 4 s, the tip of the chisel is in soft contact with the virtual object and can slide on the horizontal plane. From 5 to 7 s, the tip of the chisel is stabbing into the virtual object. In this situation, the operational force F_{vz} is less than the threshold force $-F_{s1}$. Therefore, it is difficult to slide the tip of the chisel on the horizontal plane. After 7.5 s, the pulling sensation is created by the upward force exceeding the threshold force F_{s2}, and the chisel can be moved freely. It is confirmed that the proposed control system enables the representation of the stabbing and pulling sensations.

Discussion

Table 7 shows the maximum absolute errors of positions between the virtual model and the drive system in the conventional and proposed controls on each axis. The column of 2DOF admittance control shows the results of applying the conventional [27] and proposed PD controllers to the feedback control. As seen from Table 7 , we confirmed that the tracking error of the chisel movement to the proper virtual model in the 2DOF admittance control with PD controller designed by the proposed approach is down by nearly half to that in the conventional admittance control. And, we could obtain the better tracking performance by designing systematically the PD controller with imperfect derivative. Therefore, the virtual chiseling experience by the force display device

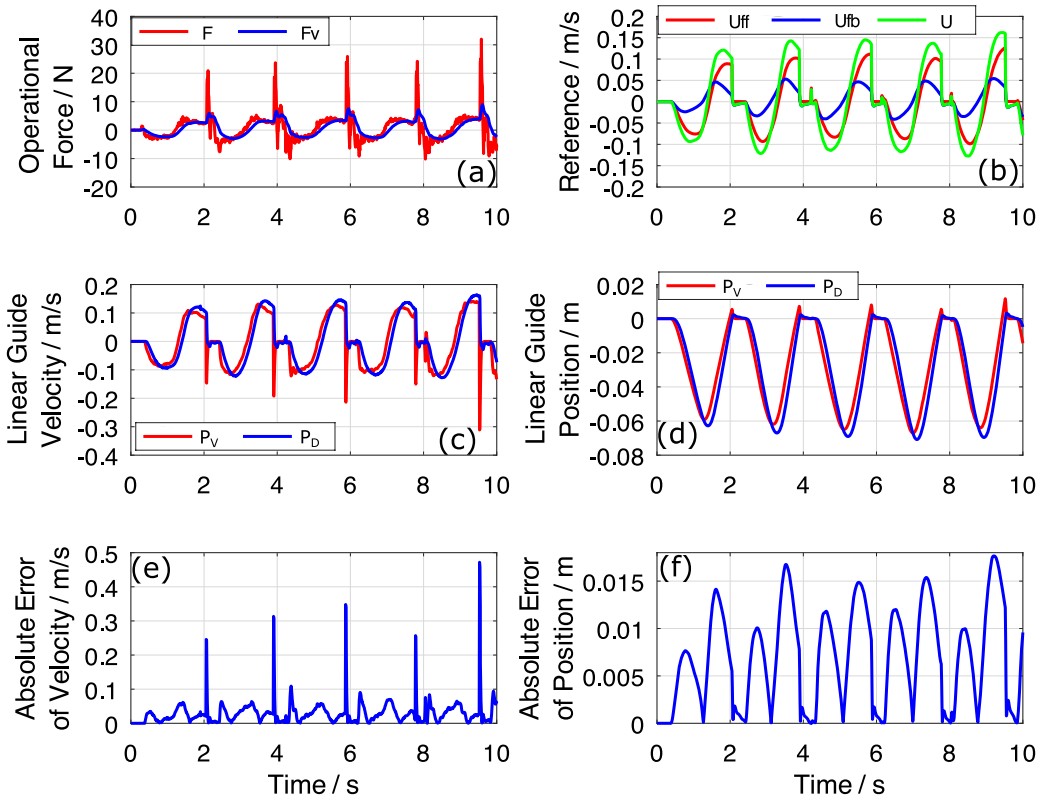

Fig. 16 Experimental results using 2DOF admittance control applied conventional PD control [27] in *y*-axis

could be improved by the proposed approach. Moreover, the gentle contact, stabbing and pulling sensations of the chiseling operation in three-dimensional space could be created by the proposed virtual model.

However, the tracking error of the drive system to the output of the virtual model is large in the situation of chisel manipulation in the air. Thus, the operator feels slightly heavy to manipulate the chisel in the air. A higher response will be required by the admittance control system to track precisely the output virtual model.

Conclusion

To virtualize the chiseling operation in the surgical training simulator in which the chisel can be used three-dimensionally, we proposed the force display device with the 2DOF admittance control system. The following conclusions are drawn from the study:

1 In the design of the feedback controller in the 2DOF admittance control system, the PD controller with imperfect derivative was designed systematically according to the frequency domain. The responsiveness of the drive system in the force display device can be improved by increasing the controller's the high frequency gain, whereas the vibrational motion in the force display device is suppressed within the allowed amplitude.

2 We proposed the virtual model of the chiseling operation in three-dimensional space that can represent the three situations of chisel manipulation in the air, contact with the hard tissue and stabbing into the hard tissue. Specifically, the stabbing situation in the proposed virtual model can represent that it is restrained to slide the chisel in the orthogonal direction to the stabbing motion.

3 In the experiments using the force display device, it was verified that the tracking performance of the drive system can be improved by the proposed 2DOF admittance control system implementing the PD controller with imperfect derivative. In addition, the soft contact, stabbing and pulling sensations of the

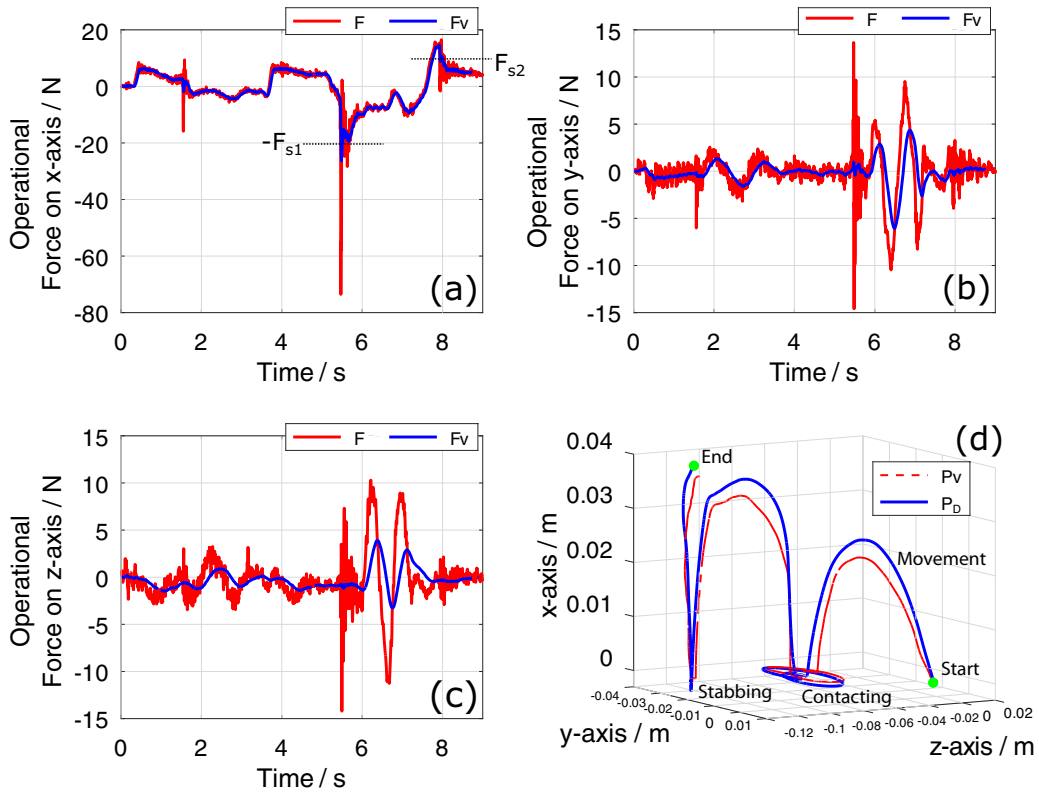

Fig. 17 Experimental results of stabbing operation using 2DOF admittance control in three-dimensional space

chiseling operation were created by the developed force display device.

In the current study, we developed the force display device for the translational chiseling operation. In future works, the rotational motion in the chiseling operation will be incorporated in the force display device. And, it is required to verify that the Coriolis force caused by the integration of translational and rotational motions can be influenced in the operational sensation.

Furthermore, to develop the surgical training simulator with high realistic sensation, it is necessary to improve the responsiveness of the drive system with respect to the force display mechanism and the control strategy.

Acknowledgements
Not applicable.

Authors' contributions
KU, YI, YK, and YN proposed the concept of the virtual training for chiseling operation. KM and YN proposed the method to enable the virtual chiseling operation. KM carried out the development of the device, programming and experiments of this study. KU, YI, and YK supported the whole development of this study. All authors read and approved the final manuscript.

Availability of data and materials
Not applicable.

Declarations

Ethics approval and consent to participate
Not applicable.

Consent for publication
Not applicable.

Competing interests
The authors declare that they have no competing interests.

Author details
[1]Integrated Graduate School of Medicine, Engineering, and Agricultural Sciences, University of Yamanashi, 4-3-11 Takeda, Kofu-shi, Yamanashi 400-8511, Japan. [2]Faculty of Engineering, Graduate Faculty of Interdisciplinary Research, University of Yamanashi, 4-3-11 Takeda, Kofu-shi, Yamanashi 400-8511, Japan. [3]Faculty of Medicine, GraduateFaculty of Interdisciplinary Research, University of Yamanashi, 1110Shimokato, Chuo-shi, Yamanashi 400-8511, Japan.

Received: 8 May 2021 Accepted: 26 August 2021
Published online: 15 September 2021

References

1. Maier J, Weiherer M, Huber M, Palm C (2020) Optically tracked and 3D printed haptic phantom hand for surgical training system. Quant Imaging Med Surg 10(2):340–355
2. Shi W, Liua PX, Zheng M (2020) Cutting procedures with improved visual effects and haptic interaction for surgical simulation systems. Comput Methods Prog Biomed 184
3. Bugdadi A, Sawaya R, Bajunaid K, Olwi D, Winkler-Schwartz A, Ledwos N, Marwa I, Alsideiri G, Sabbagh AJ, Alotaibi FE, Al-Zhrani G, Maestro RD (2018) Is virtual reality surgical performance influenced by force feedback device utilized?. J Surg Educ 76(1):262–273
4. Kim Y, Kim H, Kim YO (2017) Virtual reality and augmented reality in plastic surgery: a review. Arch Plast Surg 44(3):179–187
5. Escobar-Castillejos D, Noguez J, Neri L, Magana A, Benes B (2016) A review of simulators with haptics devices for medical training. J Med Syst 40(4)
6. Maddahi Y, Gan LS, Zareinia K, Lama S, Sepehri N, Sutherland GR (2016) Quantifying workspace and forces of surgical dissection during robot-assisted neurosurgery. Int J Med Robot Comput Assist Surg 12:528–537
7. Echegaray G, Herrera I, Aguinaga I, Buchart C, Borro D (2014) A brain surgery simulator. IEEE Comput Graph Appl 34(3):12–18
8. Lam CK, Sundaraj K, Sulaiman MN (2013) Virtual reality simulator for phacoemulsification cataract surgery education and training. Procedia Comput Sci 18:742–748
9. Wang P, Becker AA, Jones IA, Glover AT, Benford SD, Greenhalgh CM, Vloeberghs M (2007) Virtual reality simulation of surgery with haptic feedback based on the boundary element method. Comput Struct 85(7):331–339
10. Duffy AJ, Hogle NJ, McCarthy H, Lew JI, Egan A, Christos P, Fowler DL (2005) Construct validity for the lapsim laparoscopic surgical simulator. Soc Am Gastrointest Endosc Surg 19(3):401–405
11. Chen H, Sonntag CC, Mirkin KA, Pepley DF, Han DC, Moore JZ, Miller SR (2020) From the simulation center to the bedside: validating the efficacy of a dynamic haptic robotic trainer in internal jugular central venous catheter placement. Am J Surg 219(2):379–384
12. Miki T, Iwai T, Kotani K, Dang J, Sawada H, Miyake M (2016) Development of a virtual reality training system for endoscope-assisted submandibular gland removal. J Cranio-Maxillo-Fac Surg 44(11):1800–1805
13. Kovler I, Joskowicz L, Weil YA, Khoury A, Kronman A, Mosheiff R, Liebergall M, Salavarrieta J (2015) Haptic computer-assisted patient-specific preoperative planning for orthopedic fractures surgery. Int J Comput Assist Radiol Surg 10:1535–1546
14. Luciano C, Banerjee P, DeFanti T (2009) Haptics-based virtual reality periodontal training simulator. Virtual Reality 13(2):69–85
15. Łącki M, Rossa C (2020) Design and control of a 3 degree-of-freedom parallel passive haptic device. IEEE Trans Haptics 13(4):720–732
16. Hung VM, Mihai V, Dragana C, Ion I, Paraschiv N (2018) Dynamic computation of haptic-robot devices for control of a surgical training system. Int J Comput 17(2):81–93
17. Vullieza M, Zeghloula S, Khatib O (2018) Design strategy and issues of the delthaptic, a new 6-dof parallel haptic device. Mech Mach Theory 128:395–411
18. Tsumaki Y, Naruse H, Nenchev DN, Uchiyama M (1998) Design of a compact 6-dof haptic interface. IEEE Int Conf Robot Autom 3:2580–2585
19. Wijewickrema S, Copson B, Ma X, Briggs R, Bailey J, Kennedy G, O'Leary S(2018) Development and validation of a virtual reality tutor to teach clinically oriented surgical anatomy of the ear. In: IEEE international symposium on computer-based medical systems, pp 12–17
20. Chan SP, Li GL, Salisbury K, Blevins NH (2016) High-fidelity haptic and visual rendering for patient-specific simulation of temporal bone surgery. Comput Assist Surg 21(1):85-101
21. Agus M, Giachetti A, Gobbetti E, Zanetti G, Zorcolo A (2003) Real-time haptic and visual simulation of bone dissection. Prevense: Teleoperators Virtual Environ 12(1):110–122
22. Olsson P, Nysjö F, Singh NA, Thor A, Carlbom I (2015) Visuohaptic bone saw simulator: combining vibrotactile and kinesthetic feedback. Int Conf Comput Graph Interact Tech 10:1–4
23. Lin Y, Wang X, Wu F, Chen X, Wang C, Shen G (2014) Development and validation of a surgical training simulator with haptic feedback for learning bone-sawing skill. J Biomed Inform 48:122–129
24. Sofronia RE, Davidescu A, Savii GG (2012) Towards a virtual reality simulator for orthognathic basic skils. Appl Mech Mater 162:352–357
25. Masuyama K, Noda Y, Ito Y, Kagiyama Y, Ueki K (2018) Force display device and control system for surgical training simulator using bone chisel. In: IEEE International Conference on Biomedical Robotics and Biomechatronics, pp. 1248–1253
26. Masuyama K, Noda Y, Ito Y, Kagiyama Y, Ueki K (2019) Force display control system using 2 DOF admittance control in surgical training simulator with chiseling operation. In ICINCO 1:767–774
27. Masuyama K, Noda Y, Ito Y, Kagiyama Y, Ueki K (2020) Representation of chiseling operation using force display with two degree-of-freedom admittance control. Soc Instrum Control Eng 56(6):333–344 (**in Japan**)
28. The Japan Society of Mechanical Engineers (2007) Kinematics of machinery. In: Takeda Y (ed.) JSME textbook series, pp. 11–14. Maruzen Co., Tokyo (**in Japan**)
29. Alam K, Mitrofanov AV, Silberschmidt VV (2009) Finite element analysis of forces of plane cutting of cortical bone. Comput Mater Sci 46(3):738–743
30. Liao Z, Axinte DA (2016) On chip formation mechanism in orthogonal cutting of bone. Int J Mach Tools Manuf 102:41–55
31. Sui J, Sugita N (2019) Experimental study of thrust force and torque for drilling cortical bone. Ann Biomed Eng 47(3):802–812
32. Lee J, Gozen BA, Ozdoganlar OB (2012) Modeling and experimentation of bone drilling forces. J Biomech 45(6):1076–1083
33. Atkeson CG, Hollerbach JM (1985) Kinematic features of unrestrained vertical arm movements. J Neurosci 5(9):2318–2330
34. Taguchi H, Araki M (2000) Two-degree-of-freedom PID controllers—their functions and optimal tuning. IFAC Proc Vol 33(4):91–96

Publisher's Note

Terms and Conditions

Springer Nature journal content, brought to you courtesy of Springer Nature Customer Service Center GmbH (“Springer Nature”).
Springer Nature supports a reasonable amount of sharing of research papers by authors, subscribers and authorised users (“Users”), for small-scale personal, non-commercial use provided that all copyright, trade and service marks and other proprietary notices are maintained. By accessing, sharing, receiving or otherwise using the Springer Nature journal content you agree to these terms of use (“Terms”). For these purposes, Springer Nature considers academic use (by researchers and students) to be non-commercial.
These Terms are supplementary and will apply in addition to any applicable website terms and conditions, a relevant site licence or a personal subscription. These Terms will prevail over any conflict or ambiguity with regards to the relevant terms, a site licence or a personal subscription (to the extent of the conflict or ambiguity only). For Creative Commons-licensed articles, the terms of the Creative Commons license used will apply.
We collect and use personal data to provide access to the Springer Nature journal content. We may also use these personal data internally within ResearchGate and Springer Nature and as agreed share it, in an anonymised way, for purposes of tracking, analysis and reporting. We will not otherwise disclose your personal data outside the ResearchGate or the Springer Nature group of companies unless we have your permission as detailed in the Privacy Policy.
While Users may use the Springer Nature journal content for small scale, personal non-commercial use, it is important to note that Users may not:

1. use such content for the purpose of providing other users with access on a regular or large scale basis or as a means to circumvent access control;
2. use such content where to do so would be considered a criminal or statutory offence in any jurisdiction, or gives rise to civil liability, or is otherwise unlawful;
3. falsely or misleadingly imply or suggest endorsement, approval , sponsorship, or association unless explicitly agreed to by Springer Nature in writing;
4. use bots or other automated methods to access the content or redirect messages
5. override any security feature or exclusionary protocol; or
6. share the content in order to create substitute for Springer Nature products or services or a systematic database of Springer Nature journal content.

In line with the restriction against commercial use, Springer Nature does not permit the creation of a product or service that creates revenue, royalties, rent or income from our content or its inclusion as part of a paid for service or for other commercial gain. Springer Nature journal content cannot be used for inter-library loans and librarians may not upload Springer Nature journal content on a large scale into their, or any other, institutional repository.
These terms of use are reviewed regularly and may be amended at any time. Springer Nature is not obligated to publish any information or content on this website and may remove it or features or functionality at our sole discretion, at any time with or without notice. Springer Nature may revoke this licence to you at any time and remove access to any copies of the Springer Nature journal content which have been saved.
To the fullest extent permitted by law, Springer Nature makes no warranties, representations or guarantees to Users, either express or implied with respect to the Springer nature journal content and all parties disclaim and waive any implied warranties or warranties imposed by law, including merchantability or fitness for any particular purpose.
Please note that these rights do not automatically extend to content, data or other material published by Springer Nature that may be licensed from third parties.
If you would like to use or distribute our Springer Nature journal content to a wider audience or on a regular basis or in any other manner not expressly permitted by these Terms, please contact Springer Nature at

onlineservice@springernature.com